OPEN

Light trapping and surface plasmon enhanced high-performance NIR photodetector

Lin-Bao Luo[1,3], Long-Hui Zeng[1,3], Chao Xie[2,3], Yong-Qiang Yu[2,3], Feng-Xia Liang[2,3], Chun-Yan Wu[1,3], Li Wang[1,3] & Ji-Gang Hu[1,3]

[1]School of Electronic Science and Applied Physics, Hefei University of Technology, Hefei, Anhui 230009, P. R. China, [2]School of Materials Science and Engineering, Hefei University of Technology, Hefei, Anhui 230009, P. R. China, [3]Anhui Provincial Key Laboratory of Advanced Functional Materials and Devices, Hefei University of Technology, Hefei, Anhui 230009, P. R. China.

Heterojunctions near infrared (NIR) photodetectors have attracted increasing research interests for their wide-ranging applications in many areas such as military surveillance, target detection, and light vision. A high-performance NIR light photodetector was fabricated by coating the methyl-group terminated Si nanowire array with plasmonic gold nanoparticles (AuNPs) decorated graphene film. Theoretical simulation based on finite element method (FEM) reveals that the AuNPs@graphene/CH_3-SiNWs array device is capable of trapping the incident NIR light into the SiNWs array through SPP excitation and coupling in the AuNPs decorated graphene layer. What is more, the coupling and trapping of freely propagating plane waves from free space into the nanostructures, and surface passivation contribute to the high on-off ratio as well.

S ilicon (Si) with an indirect narrow band-gap (~1.12 eV), has been central to numerous technological innovations for decades and remains to be the irreplaceable key material for electronic industry[1,2]. Compared with their thin film and bulk counterparts, silicon nanowires (SiNWs) with large surface-to-volume ratio[3], and superior transport property[4], have shown intriguing potential as functional building block for fabricating various optoelectronic devices, such as field-effect transistors[5], solar cell[6], chemical and biologic sensors[7,8], photodetectors (PDs)[9], and so on. Among various SiNWs-based nano-devices, PDs assembled from Si nanostructures have received special research interests[10,11]. By virtue of the appropriate band-gap and enhanced optical properties, SiNWs-based PDs are able to probe infrared light with high sensitivity and excellent photo-response, which can constitute the core component for large-scale applications in many areas such as military surveillance, target detection and tracking[12]. In order to further boost the device performance (e.g. on/off ratio, response speed) of SiNWs-based PDs, people are resorting to new device structures with suppressed carrier recombination, enhanced light absorption and carrier transportation.

Graphene, as a promising alternative to transparent electrode, has exhibited extraordinary properties such as high optical transmittance, high thermal conductivity, excellent electronic and mechanical properties, as well as outstanding chemical/physical stability with tunable work function[13]. As a result, graphene has been widely utilized in various photovoltaic devices[14], PDs[15], and light-emitting diodes (LEDs)[16]. Surface plasmons (SPs), the electromagnetic wave induced electrical charges collective oscillation at the surfaces of metals is the pillar stones of application in light trapping[17,18]. Plasmonic noble metal nanoparticles (e.g. Au, Ag NPs) decorated graphene emerges as an alternative, unique electrode material that displays a wide range of extraordinary properties[19], including strong absorption of light in NIR and visible range and supporting the surface plasmon polaritons (SPPs) in graphene. Additionally, SPPs bound to the surface of graphene exhibits unique features such as high modal index, relatively low loss, and flexible tunability by electric field, and magnetic field[20,21]. Herein, we propose a simple strategy to fabricate high-performance NIRPDs by coating SiNWs array with AuNPs decorated graphene. The as-fabricated device exhibits obvious sensitivity to 850 nm light illumination with an on/off ratio of 10^6, the highest value compared with other Si based devices. Theoretical simulation based on finite element method (FEM) reveals that the high performance can be ascribed to the excellent optical property of AuNPs@ graphene/SiNWs array which as a highly efficient SPP-based NIR light coupling system, is capable of trapping the incident NIR light into the SiNWs array through SPP excitation and coupling in the AuNPs decorated graphene

layer. The generality of the above result suggests that our NIRPD will have potential application in future optoelectronic devices.

Results

The scheme in Fig. 1a illustrates the procedures to fabricate the AuNPs@graphene/SiNWs array NIRPD. The vertical SiNWs array synthesized *via* a Ag-assisted chemical etching method was methyl-terminated to reduce charge recombination at the surface of the SiNWs. The polymethylmethacrylate (PMMA)-supported multi-layer graphene film was then transferred onto the surface of the SiNWs array, followed by removal of the PMMA in acetone. Finally, AuNPs were deposited onto graphene by spin-coating $AuCl_3$ solution. Fig. 1b shows the cross-sectional SEM image of SiNWs array, from which well-aligned SiNWs with length of about $28 \sim 30$ μm were observed. According to the statistical distribution in Fig. 1c, the diameters of the SiNWs are in the range of 120–220 nm, with an average value of ~170 nm. Raman spectrum of the graphene film is found to consist of two sharp peaks: i.e., 2D-band peak at ~2698 cm^{-1} and G-band peak at ~1581 cm^{-1}. The intensity ratio of $I_{2D} : I_G \approx 1.02$, and the presence of weak D-band scattering at ~1350 cm^{-1}, suggest that the graphene is mainly composed of multilayer graphene with few defects (Fig. 1d)[22,23]. Fig. 1g depicts a representative SEM image of multilayer graphene/SiNWs Schottky junction which is modified by AuNPs with diameters in the range of 40–100 nm. These AuNPs, uniformed dispersed on the graphene film (Fig. 1e), are formed through the reduction of Au ions by accepting electrons from graphene (c.f. Fig. 1f)[24].

In this study, the SiNWs array was intentionally functionalized by monolayer methyl-group such that the surface recombination can be effectively suppressed[25]. Fig. 2a shows the current-voltage (I-V) curves

of a typical AuNPs@graphene/SiNWs array device at room temperature, from which one can see that the device exhibits obvious rectifying behavior due to the presence of Schottky barrier between graphene and SiNWs. Fig. 2b compares the current density – voltage (J-V) curves of three samples with and without surface functionalization. It can be easily seen that, with the illumination of a NIR light ($\lambda = 850$ nm, 3 mW/cm²), the AuNPs@graphene/SiNWs array structure exhibits the best photovoltaic characteristics in terms of open circuit voltage (V_{oc}) and short circuit current density (J_{sc}). Remarkably, such a photovoltaic effect can allow the efficient sensing of NIR light. As illustrated in Fig. 2c, when the light was turned on and off alternately at zero bias voltage, the AuNPs@graphene/SiNWs array can be reversibly switched between low- and high-resistivity states with a dark current of (I_{dark}) 4.1 pA, and a photocurrent (I_{light}) of 27 μA, yielding an I_{light}/I_{dark} ratio $>10^6$, the highest value among the three samples (see Fig. 2c and Fig. S1). As we will discuss later, this high on-off ratio could be partially attributed to the enhanced optical absorption of the NIRPD after decoration of the plasmonic AuNPs. Moreover, the increased sheet conductivity of the graphene electrode after decoration with AuNPs can be also contributed to the high on-off ratio as it can substantially reduce the series resistance in the circuit. Fig. 2d depicts the spectral response of three devices, it is clear that the spectral response of these three devices displays virtually similar spectral selectivity, with peak sensitivity at around 950 nm.

Discussion

The photocurrent of the current NIRPD displays high dependence on the intensity of excitation light. Fig. 3a plots the photocurrent of AuNPs@graphene/SiNWs array NIRPD under light illumination
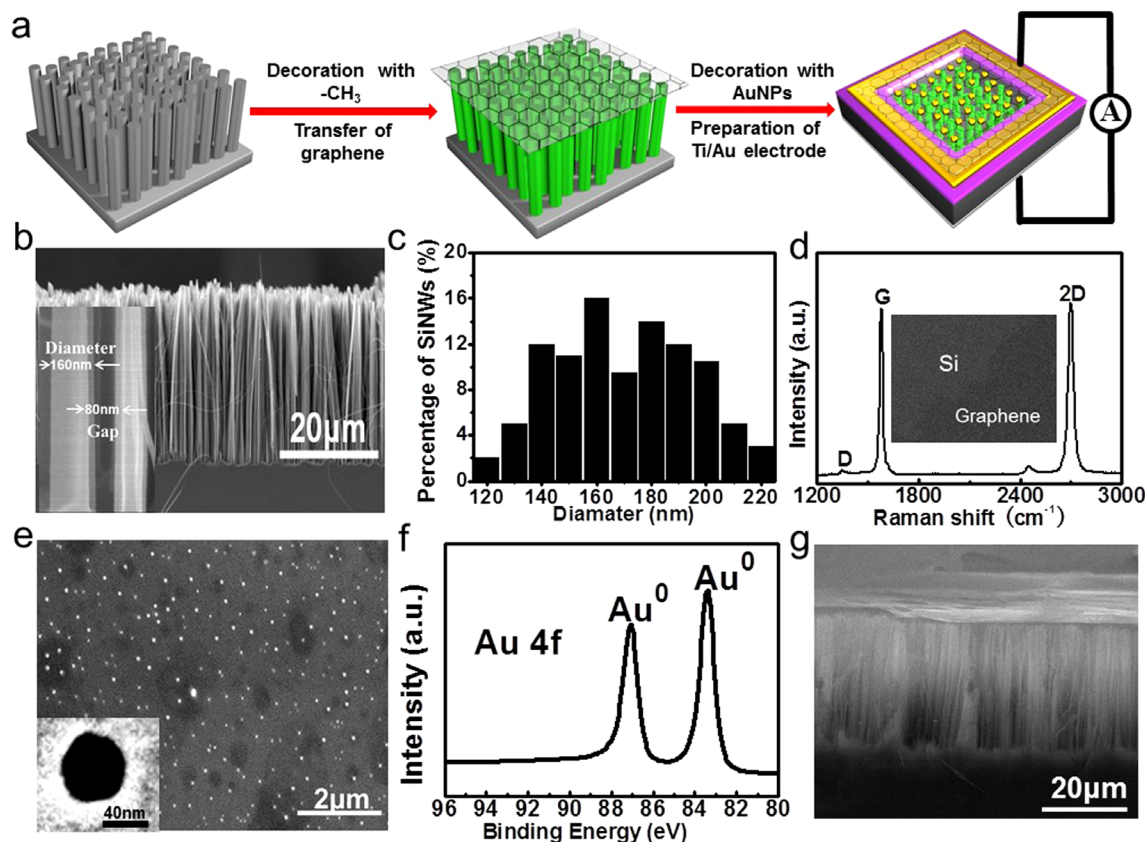

Figure 1 | Device fabrication and structure characterization. (a) Schematic illustration of the step-wise process for fabrication of the NIRPD; (b) Cross-sectional SEM image of the SiNWs, the inset shows the magnified SEM image of the SiNWs array; (c) Statistical distribution of the diameters of SiNWs; (d) Raman spectrum of the multilayer graphene film, the inset shows a SEM image of the graphene film on the Si substrate; (e) SEM image of AuNPs on graphene film, the inset shows TEM image of a AuNP; (f) The Au 4f spectrum of AuNPs on the graphene film; (g) Cross-sectional SEM image of NIRPD.
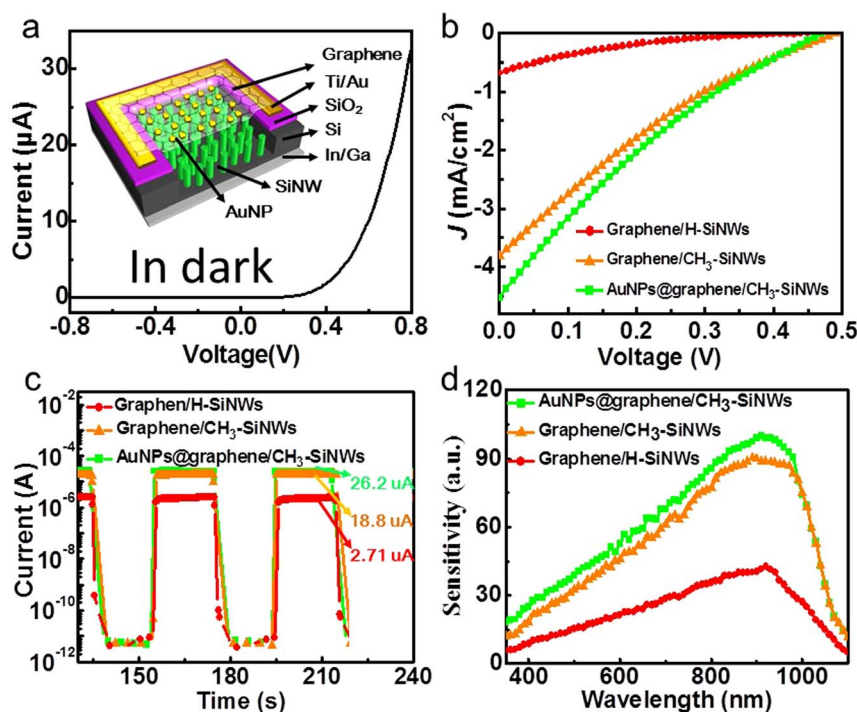
Figure 2 | Optoelectronic characteristics of the NIRPD. (a) *I-V* curves of the NIRPD measured at room temperature, the inset shows the device structure; (b) *I-V* characteristics, and (c) photoresponse of three representative devices under 850 nm light illumination at $V_{bias} = 0$ V; (d) The corresponding spectral response, the sensitivity is defined by $100 \times I_{current}/I_{max}$, where I_{max} is the maximum photocurrent of AuNPs@graphene/CH_3-SiNWs array, at around 950 nm. To make the analysis more reliable, we kept the light power identical for all wavelengths during analysis.

with different intensities. It is obvious that the photocurrent of the device increases gradually with increasing light intensity. This dependence of photocurrent on light intensity can be fitted by a simple power law: $i_{photo} = AP^\theta$, where A is a constant for a certain wavelength, and the exponent θ ($0.5 < \theta < 1$) determines the response of photocurrent to light intensity[26]. By fitting this equation, θ is estimated to be 0.91. This nearly integer exponent suggests that the trap states have been effectively lessened which is highly beneficial to the photosensing ability[27]. Next, the photoresponse of the NIRPD to pulsed IR light (850 nm) was also investigated. As shown in Fig. 3d, for all switching frequencies (0–2200 Hz), our device can be reversibly switched between high and low conductance. Notably, even at 2200 Hz, the relative balance only decreases by less than 10%, indicating great potential to monitor pulsed light with very high frequency. As shown in Fig. 3e, the response time is defined as the time required for the photocurrent to increase from 10% to 90%, the recovery time is defined analogously. Careful analysis of curve leads to a small response/recovery time (τ_r/τ_f) of 73/96 μs in switching frequency of 2200 Hz. This response speed is much quicker than that of similar PDs (c.f. Table 1). We believe the fast response speed can be attributed to the following two factors: (1) The built-in electric field formed by the Schottky junction. During light detection, the photo-excited electron-hole pairs can be quickly separated by the electric field and then transferred to the electrodes, giving rise to fast response speed. (2) Effective surface passivation of SiNWs surface. The surface energy band bending caused by the -CH_3 modification can also facilitate the separation of photo-generated electron-hole pairs in the radial direction of SiNWs.

In order to clearly compare the performance of our device with existing counterparts, the responsivity (R) and detectivity (D^*), two key metrics normally used to quantify the performance of photodetector are calculated. For the present NIRPD, the responsivity and detectivity were calculated to be 1.5 A/W and 2.54×10^{14}, respectively (Please refer to the supporting information for the detailed calculation of both parameters). Table 1 summarizes the device per-

formance of the present device and other PDs with similar structures. Although the responsivity does not show any obvious advantage, the detectivity of the present device shows the highest value, and the response/recovery time of our device is substantially reduced, in comparison with other Si based NIRPDs. What is more, the on/off ratio is much higher than not only graphene/ZnO nanorods array[28], graphene/Ge wafer[29], graphene-PbS quantum dot (QDs)[30], graphene QDs arrays[31], and graphene/CdSe nanobelt PDs[32], but also Si based photodetector including graphene/Si substrate (10^4)[2] and pure graphene/SiNWs heterojunction $(\sim10^3)$[33].

To unveil the physics behind the high performance of NIRPD, we studied the optical properties of AuNPs@graphene/SiNWs array structure using FEM. For the sake of convenience, we only consider the graphene/SiNWs at first. Under the illumination of 850 nm light, the equivalent relative permittivity of graphene sheet can be obtained by Kumbo formula as $-0.6245 + 0.0015i$ (see details in the supporting information), where the negative real part and near-zero imaginary part of epsilon suggests that it behaves as a low-loss transparent metal film. These unique electrical and optical characteristic enable the dual-function for the graphene sheet, i.e., serving as both excellent transparent electrode and metallic thin film for SPP excitation. Fig. 4a–h illustrate the electric field energy distribution of the graphene/SiNWs array with average period and diameter of 220 and 140 nm, 240 and 160 nm, 260 and 180 nm, 280 and 200 nm. It is visible that incident light can be efficiently coupled into the SiNWs. Such a light trapping effect is so efficient that the field intensity is very high even in the NW, ~4 μm away from the Schottky contact, leading to the high energy utilization efficiency. Specifically, according to the magnified electric field energy distribution (Fig. 4b, d, f, h), the strongest electric field can be induced by the SiNWs with a diameter 180 nm, which agrees with the average diameter of the as-etched SiNWs. Moreover, waves with the large wave vector provided by the scattering in the process of end-coupling can excite the SPP waves in the graphene layer, leading to apparent electric field enhancement, which can greatly facilitate the improvement of electron transport
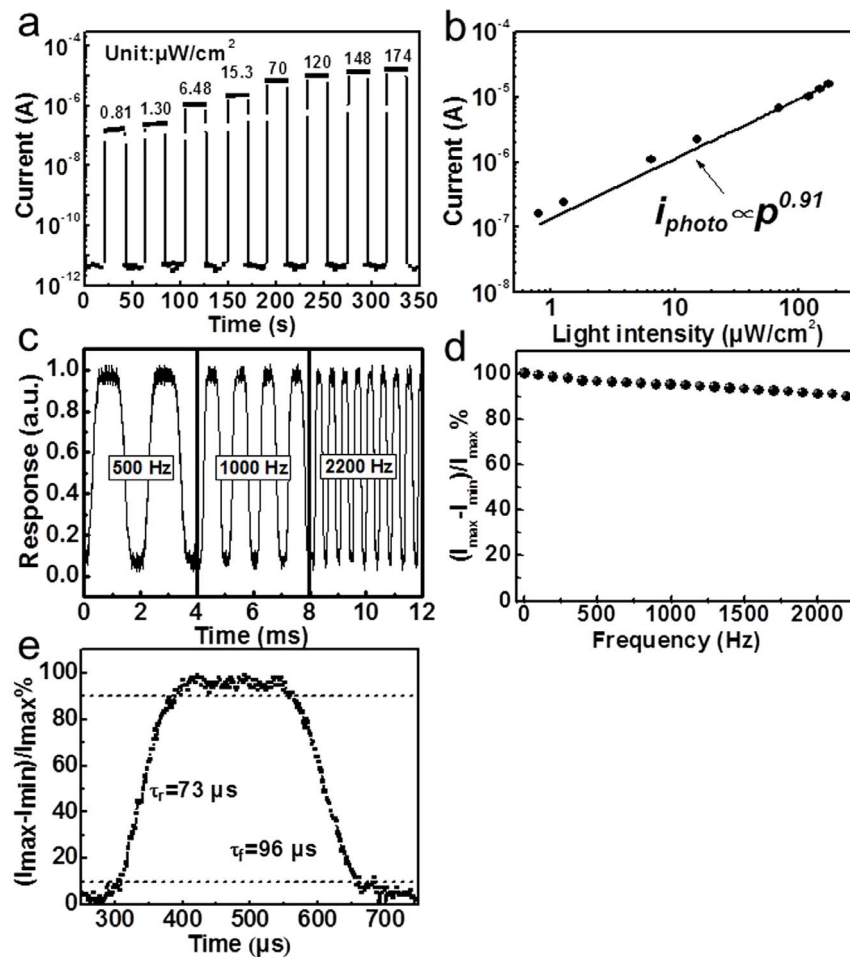
Figure 3 | Photoresponse of the NIRPD. (a) Photoresponse of the AuNPs@graphene/CH$_3$-SiNWs array NIRPD under light illumination with increasing intensities from 0.81 to 174 μW/cm^2; (b) The fitting of the relationship between the photocurrent and light intensity. The light wavelength was 850 nm; (c) Photoresponse of the NIRPD to pulsed IR light irradiation (850 nm) at different frequencies; (d) The relative balance $(I_{max} - I_{min})/I_{max}$ versus switching frequency; (e) A single normalized cycle measured at 2200 Hz for estimating both response time (τ_r) and recovery time (τ_f).

efficiency at the interface between the graphene sheet and SiNWs. This excellent optical property is in stark contrast to the case of bulk Si/graphene. Fig. 5a shows the poor field penetration depth and intensity in bulk Si layer. It can be observed that most of the light will be reflected at the incident interface, and no SPP waves are generated due to unmatched moment between incident light in free space and SPP waves in graphene sheet[34,35]. As matter of fact, this theoretical simulation result is in good agreement with the reduced reflectivity, as illustrated in Fig. 5b. The effective light trapping effect and remarkable SPP-induced field enhancement at top interface offered by the graphene/SiNWs array structure are highly beneficial to the IR light detection as they can provide a long optical path and more surface area for efficient light harvesting, enhancing light coup-

ling efficiency from free space to SiNWs, and suppress light reflection[36].

Interestingly, the light trapping efficiency and localized field spatial distribution of the graphene/SiNWs array junction can be further enhanced through the introduction of the plasmonic AuNPs on the surface of multilayer graphene layer. In this case, the AuNPs@graphene/SiNWs array is virtually an SPP-based light coupling regime in which the AuNPs can act as sub-wavelength scattering elements to couple and trap freely propagating plane waves from free space into an absorbing semiconductor structure by forward scattering the light into the nanowires[17]. Furthermore, SPPs excited at the AuNPs/graphene interface can efficiently trap and guide light into the SiNWs. Fig. 6a–d show the simulated electric field energy distribution of the

| Table 1	Summary of the device performances of the present NIRPD and other photodetectors with similar device structures				
Device Structure	Responsivity (A/W)	Response/Recovery time	I_{light}/I_{dark}	Detectivity (Jones)	Ref
AuNPs@graphene/CH$_3$-SiNWs	1.5	73/96 μs	~10^6	~10^{14}	Our work
graphene/Si	0.435	1.2/3 ms	~10^4	~10^8	2
graphene/ZnO nanorods array	113	0.7/3.6 ms	~10^3	/	28
graphene/Ge wafer	0.05	23/108 μs	~10^4	~10^{10}	29
graphene-PbS QDs	10^7	10/10 ms	/	~10^{13}	30
graphene QDs arrays	8.61	/	~10^1	/	31
graphene/n-CdSe nanobelt	8.7	70/137 μs	~10^5	/	32
graphene/pure SiNWs	/	20 ms	~10^3	/	33
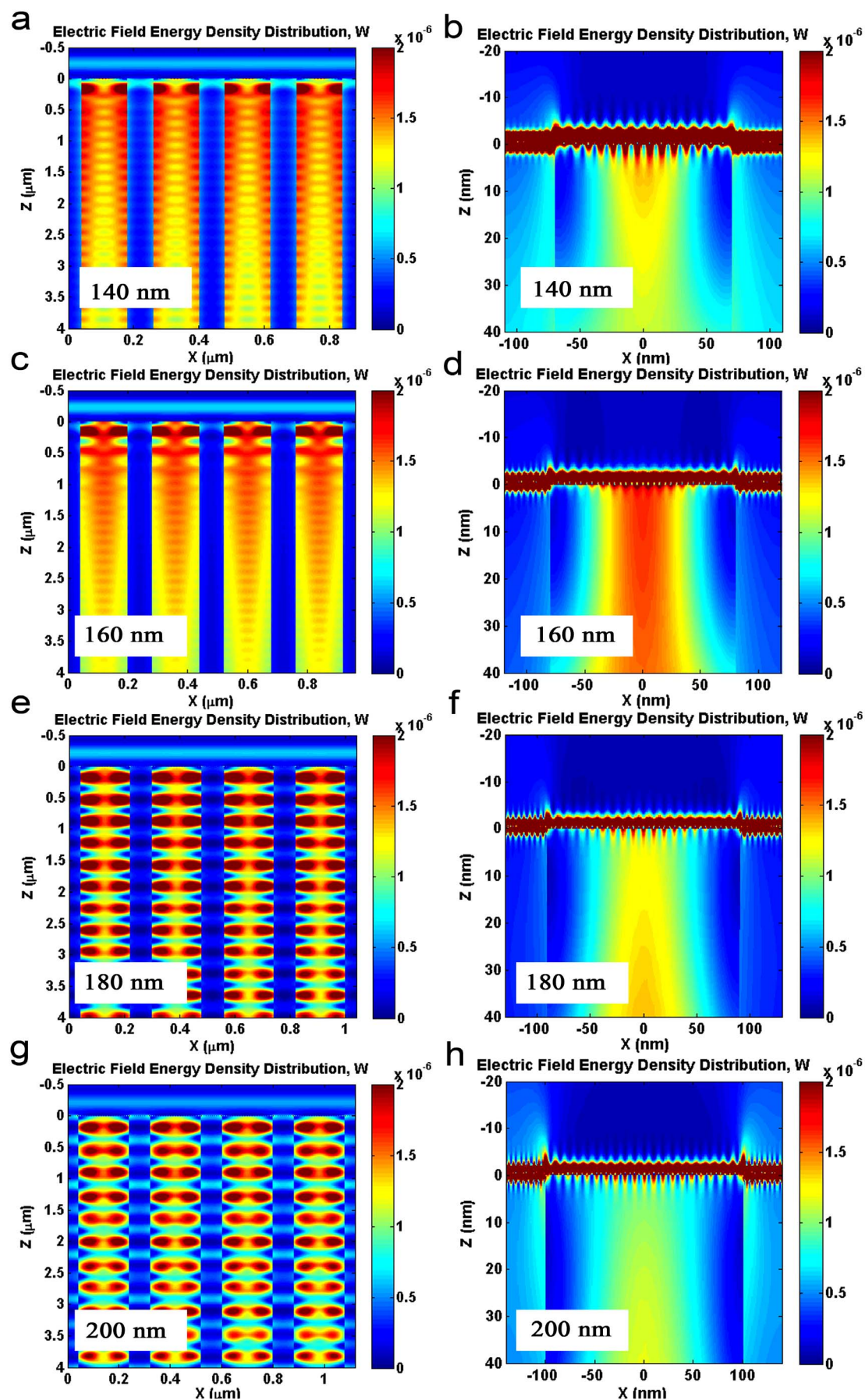
Figure 4 | Theoretical simulation of graphene/SiNWs array structure. Simulated electric field energy distribution for the graphene/SiNWs with average period and diameter of (a) 220 and 140 nm, (c) 240 and 160 nm, (e) 260 and 180 nm and (g) 280 and 200 nm; (b), (d), (f) and (h) show the magnified electric field energy distribution of one unit of graphene/SiNWs. The average value of the gap between two adjacent SiNWs is ~80 nm.
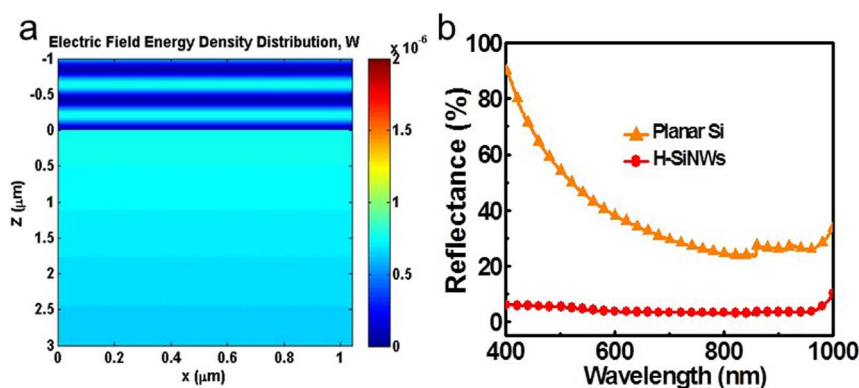
Figure 5 | Optical properties of the planar Si and H-SiNWs. (a) The electric field energy distribution of bulk Si with graphene layer. (b) Reflection spectra of both planar Si and H-SiNWs array.

devices with AuNPs of different diameters, from which one can see that the strong coupling between the AuNPs and graphene sheet makes the SPP localized field more concentrated in the area just below the AuNPs[37]. Notably, relatively strong localized filed can be observed in the coupling system composed of graphene and AuNPs with diameter in the range of 60–70 nm. Such a special feature can not only cause increased field enhancement in graphene sheet, but also lead to directional scattering and coupling of light into the
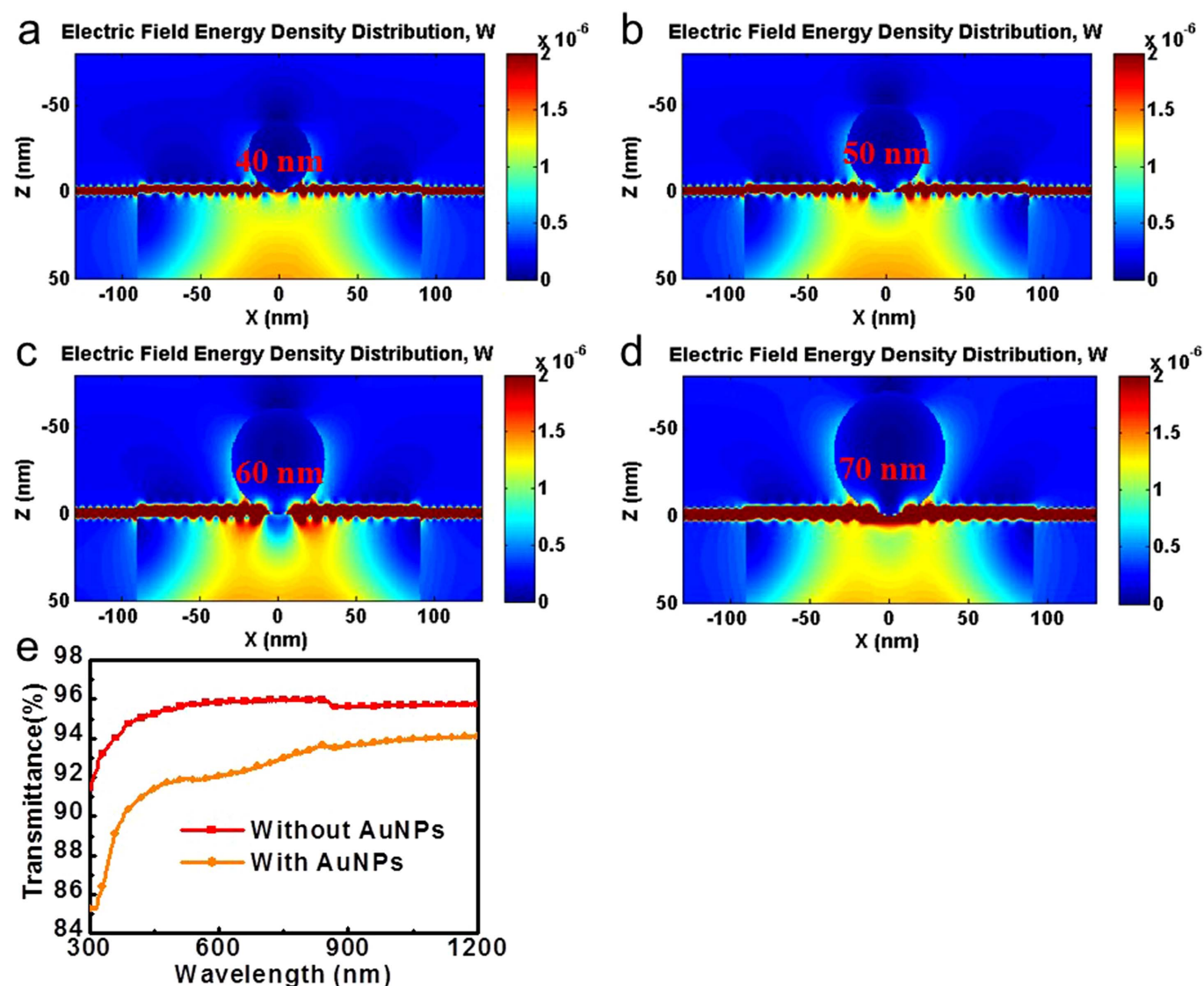

Figure 6 | Simulated electric field energy distribution of the NIRPDs. The diameters of the AuNPs are 40 nm (a), 50 nm (b), 60 nm (c) and 70 nm (d), respectively. Note that the period and diameter of SiNWs are 260 and 180 nm, respectively. (e) The transmittance of graphene with and without Au decoration.
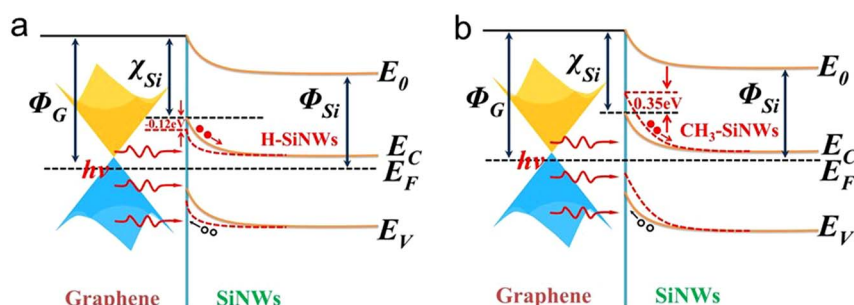
Figure 7 | Working mechanism of the AuNPs@graphene/SiNWs array NIRPD. Energy band diagrams of before (a), and after surface modification (b); the Φ_G/Φ_{Si} denote the work functions of graphene/SiNWs, respectively, E_C and E_V are the conduction band minimum and valence band maximum of Si, respectively, E_F, χ_{Si} and E_0 are the Fermi energy level, the electron affinity of Si, and the vacuum energy level, respectively.

SiNWs under the AuNPs. This improvement in light trapping efficiency and localized field enhancement agrees well with transmittance spectrum shown in Fig. 6e.

Apart from the SPPs-induced light trapping effect, the surface modification of SiNWs contributes to the enhancement of device performance as well. Fig. 7 illustrates the energy band diagrams of the graphene/SiNWs Schottky junction before and after surface modification. It is noted that surface modification can considerably alter the surface electron affinity of SiNWs: The offset of surface electron affinity for the CH_3-SiNWs could be as high as $+0.35$ eV, while it is -0.12 eV for H-SiNWs without CH_3-termination[38]. Therefore, the built-in electric field was greatly strengthened in the CH_3-SiNWs device, as compared with the H-SiNWs device. On the other hand, the surface energy band bending caused by the -CH_3 modification can also facilitate the separation of photogenerated electron-hole pairs in the radial direction of SiNWs; the holes will accumulate on the NW surface while electrons in the NW core, preventing the carrier recombination. Thirdly, passivation of surface states *via* Si-C on the SiNWs surface decreases the probability of electron-hole combination and thus increases the carrier mobilities[39]. As a result, the lifetime of the minority carrier (holes) in the SiNWs will be prolonged, giving rise to increased photocurrent.

In summary, high-performance NIRPD have been successfully fabricated by coating the surface of graphene/SiNWs array with plasmonic AuNPs. The on/off ratio can reach as high as 10^6, the highest value ever reported. In addition, the responsivity and detectivity at zero bias voltage were estimated to be 1.5 AW^{-1}, and 2.52×10^{14} $cmHz^{1/2}W^{-1}$, respectively. Further device analysis shows that the NIRPD can work in a wide range of chopping frequencies, with high response speed (response/recovery time of 73/96 μs). Theoretical simulation based on FEM reveals that the high sensitivity is mainly attributed to light trapping and remarkable SPP-induced field enhancement. Moreover, the coupling and trapping of freely propagating plane waves from the light into the absorbing semiconductor structure, and efficient surface passivation of the SiNWs also contribute to the observed high performance.

Methods

Preparation and characterization of SiNWs array and graphene. The vertical SiNWs array in this work was prepared using a Ag-assisted chemical etching approach. Briefly, windows with size of 0.2×0.25 cm² were first defined on the SiO₂ (300 nm)/*n*-Si wafers (resistivity: 1–10 Ωcm) substrates by adhesive tape, followed by dipping into a buffered oxide etch (BOE) solution until the underlying Si substrates were exposed. The as-obtained substrate was then immersed into a mixed solution of HF (4.8 M) and AgNO₃ (0.005 M) to coat AgNPs, which will act as catalyst during etching in the etchant composed of HF (4.8 M) and H₂O₂ (0.4 M). After etching for 20 min, the as-obtained SiNWs array were dipped into a diluted HNO₃ and HF solution to dissolve Ag and SiO₂ on the surface of SiNWs array, respectively. Methyl group-terminated SiNWs array (denoted as CH_3-SiNWs) was prepared following a two-step chlorination/alkylation method[25]. The multilayer graphene film was grown on 20 μm thick Cu foil at 1000°C *via* a chemical-vapor deposition (CVD) method[40]. After growth, the graphene films were spin-coated with 5 wt.% polymethylmethacrylate (PMMA) in chlorobenzene, and then the underlying Cu foil

were removed in Marble's reagent solution ($CuSO_4 : HCl : H_2O =$ 10 g : 50 ml : 50 ml). The graphene film was rinsed in deionized water to remove the remaining ions. The multilayer graphene films were directly transferred onto SiO₂/Si substrate and the PMMA was removed by acetone. The chemical composition of the AuNPs decorated graphene was analyzed by X-ray photoemission spectroscopy (XPS) which was performed on a VG ESCALAB 220i-XL analysis system equipped with a monochromatic Al x-ray (1486.6 eV) source.

Device construction and evaluation. To fabricate the AuNPs decorated graphene/SiNWs Schottky junction photodetector, 5/50 nm Ti/Au electrode, which served as the electrical contact for graphene, was first deposited on the SiO₂/Si substrate using electron-beam evaporator. Then the PMMA-supported multilayer graphene films were directly transferred onto the top of SiNWs. After drying at 100°C for 10 min, the residual PMMA on graphene film was removed by acetone. Indium-gallium (In-Ga) alloy was then pasted on the rear side of Si subatrate to achieve ohmic contact. AuNPs on graphene was obtained by spin-coating of AuCl₃ (10 mM in nitromethane) onto the substrate at 2000 rpm for 1 min. The device characteristics of graphene/SiNWs were measured using a Keithley 4200 semiconductor characterization system. To determine the spectral response and time response of the Schottky junction devices, a home-built system composed of a light source (LE-SP-LS-XE), a monochromator (LE-SP-M300), an oscilloscope (Tektronix, TDS2012B), and an optical chopper (LE-oc120) was used.

Theoretical simulation. The simulation of electric field energy density distribution was performed by the finite element method (FEM). In our calculation, the incident light is *p*-polarized with a wavelength of 850 nm, and the permittivity of Si and Au are $13.410 + 0.029i$ and $-28.168 + 1.752i$[41,42], respectively. The equivalent relative permittivity of graphene can be determined by the formula $\varepsilon_G = 1 + \frac{i\sigma_G \eta_0}{k_0 d}$, in which the multilayered graphene is treated as an ultra-thin film with thickness of ~1 nm, i is the pure imaginary, η_0 and k_0 are the impedance and wave vector in air, respectively. The conductivity σ_G is determined by Kumbo formula[43,44], and can be evaluated as[45,46]

$$\sigma_G = i \frac{e^2 k_B T}{\pi \hbar^2 (\omega + i\tau^{-1})} \left\{ \frac{\mu_c}{k_B T} + 2\ln[\exp(-\frac{\mu_c}{k_B T}) + 1] \right\} \quad (1)$$

where ω is the light angular frequency, T the temperature, e the electron charge, $\hbar$ the reduced Planck's constant, k_B the Boltzmann constant, μ_c and τ the chemistry potential and the momentum relaxation time, respectively. Specifically, under $\lambda = 850$ nm (1.459 eV), $T = 300$ K, $\mu_c = 0.12$ eV and $\tau = 0.5$ ps, the equivalent relative permittivity of graphene is estimated to be $-0.6245 + 0.0015i$, suggesting a metal-like behavior and little optical loss.

1. Sze, S. M. & Ng, K. K. [Physics and properties of semiconductors-a review] *Physics of semiconductor devices* 7–8 (John Wiley & Sons, Inc., New Jersey, 2006).
2. An, X. H., Liu, F. Z., Jung, Y. J. & Kar, S. Tunable graphene-silicon heterojunctions for ultrasensitive photodetection. *Nano Lett.* **13**, 909–916 (2013).
3. Patolsky, F., Zheng, G. F. & Lieber, C. M. Fabrication of silicon nanowire devices for ultrasensitivie, label-free, real-time detection of biological and chemical species. *Nat. Protoc.* **1**, 1711–1724 (2006).
4. Cui, Y., Zhong, Z. H., Wang, D. L., Wang, W. U. & Lieber, C. M. High performance silicon nanowire field effect transistor. *Nano Lett.* **3**, 149–152 (2003).
5. Wu, Y. *et al.* Controlled growth and structures of molecular-scale silicon nanowires. *Nano Lett.* **4**, 433–436 (2004).
6. Kelzenberg, M. D. *et al.* Photovoltaic measurements in single-nanowire silicon solar cells. *Nano Lett.* **8**, 710–714 (2008).
7. Cui, Y., Wei, Q. Q., Park, H. K. & Lieber, C. M. Nanowire nanosensors for highly sensitive and selective detection of biological and chemical species. *Science* **293**, 1289–1292 (2001).
8. Luo, L. B. *et al.* Silicon nanowire sensors for Hg²⁺ and Cd²⁺ ions. *Appl. Phys. Lett.* **94**, 193101 (2009).

9. Zhang, A., Kim, H. K., Cheng, J. & Lo, Y. H. Ultrahigh responsivity visible and infrared detection using silicon nanowire phototransistors. *Nano Lett.* **10**, 2117–2120 (2010).

10. Yang, C., Barrelet, C. J., Capasso, F. & Lieber, C. M. Single p-type/intrinsic/n-type silicon nanowires as nanoscale avalanche photodetectors. *Nano Lett.* **6**, 2929–2934 (2006).

11. Mulazimoglu, E. *et al.* Silicon nanowire network metal-semiconductor-metal photodetector. *Appl. Phys. Lett.* **103**, 083114 (2013).

12. Rogalski, A. Infrared detectors: An overview. *Infrared Phys.Technol.* **43**, 187–210 (2002).

13. Lee, C. G., Wei, X. D., Kysar, J. W. & Hone, J. Measurement of the elastic properties and intrinsic strength of monolayer graphene. *Science* **321**, 385–388 (2008).

14. Kavan, L., Yum, J. H. & Gratzel, M. Graphene nanoplates outperforming platinum as the electrocatalyst in co-bipyridine-mediated dye-sensitized solar cell. *Nano Lett.* **11**, 5501–5506 (2011).

15. Wang, M. Z. *et al.* TiO$_2$ nanotube array/monolayer graphene film Schottky junction ultraviolet light photodetectors. *Part. Part. Syst. Charact.* **30**, 630–636 (2013).

16. Ye, Y. *et al.* Multicolor graphene nanoribbon/semiconductor nanowire heterojunction light-emitting diodes. *J. Mater. Chem.* **21**, 11760–11763 (2011).

17. Atwater, H. A. & Polman, A. Plasmonics for improved photovoltaic devices. *Nat. Mater.* **9**, 205–213 (2010).

18. Liu, N. *et al.* Plasmonic Amplification with Ultra-High Optical Gain at Room Temperature. *Sci. Rep.* **3**, 1967; DOI:10.1038/srep01967 (2013).

19. Koppens, F. H. L., Chang, D. E. & Javier García de Abajo, F. Graphene plasmonics: A platform for strong light–matter interactions. *Nano Lett.* **11**, 3370–3377 (2011).

20. Wang, B., Zhang, X., García-Vidal, F. J., Yuan, X. C. & Teng, J. H. Strong coupling of surface plasmon polaritons in monolayer graphene sheet arrays. *Phys. Rev. Lett.* **109**, 073901 (2012).

21. Lee, C. G., Wei, X. D., Kysar, J. W. & Hone, J. Measurement of the elastic properties and intrinsic strength of monolayer graphene. *Science* **321**, 385–388 (2008).

22. Ferrari, A. C. *et al.* Raman spectrum of graphene and graphene layers. *Phys. Rev. Lett.* **97**, 187401 (2006).

23. Ni, Z. H. *et al.* Graphene thickness determination using reflection and contrast spectroscopy. *Nano Lett.* **7**, 2758–2763 (2007).

24. Gűnes, F. *et al.* Layer-by-layer doping of few-layer graphene film. *ACS Nano* **4**, 4595–4600 (2010).

25. Zhang, X. Z. *et al.* High-efficiency graphene/Si nanoarray Schottky junction solar cells via surface modification and graphene doping. *J. Mater. Chem. A.* **1**, 6593–6601 (2013).

26. Joshi, N. V. [Transient photoconductivity] *Photoconductivity: art science and technology* 77–111 (Marcel Dekker, Inc., New York, 1990).

27. Kung, S. C., van der Veer, W. E., Yang, F., Donavan, K. C. & Penner, R. M. 20 μs photocurrent response from lithographically patterned nanocrystalline cadmium selenide nanowires. *Nano Lett.* **10**, 1481–1485 (2010).

28. Nie, B. *et al.* Monolayer graphene film on ZnO nanorod array for high-performance Schottky junction ultraviolet photodetetors. *Small* **9**, 2872–2879 (2013).

29. Zeng, L. H. *et al.* Monolayer graphene/germanium Schottky junction as high-performance self-driven infrared light photodetector. *ACS Appl. Mater. Interface.* **5**, 9362–9366 (2013).

30. Konstantatos, G. *et al.* Hybrid graphene-quantum dot phototransistors with ultrahigh gain. *Nat. Nano.* **7**, 363–368 (2012).

31. Zhang, Y. Z. *et al.* Broadband high photoresponse from pure monolayer graphene photodetector. *Nat. Commun.* **4**, 1811 (2013).

32. Jin, W. F. *et al.* Self-powered high performance photodetectors based on CdSe nanobelt/graphene Schottky junctions. *J. Mater. Chem.* **22**, 2863–2867 (2012).

33. Xie, C. *et al.* Schottky solar cells based on graphene nanoribbons/multiple silicon nanowires junction. *Appl. Phys. Lett.* **100**, 193103 (2012).

34. Barnes, W. L., Dereux, A. & Ebbesen, T. W. Surface plasmon subwavelength optics. *Nature* **424**, 824–830 (2003).

35. Raether, H. [Surface plasmons on smooth surfaces] *Surface plasmons on smooth and rough surfaces and on gratings* 4–37 (Springer, Berlin, 1988).

36. Fan, G. F. *et al.* Graphene/silicon nanowire Schottky junction for enhanced light harvesting. *ACS Appl. Mater. Interface.* **3**, 721–725 (2011).

37. Mubeen, S. *et al.* Plasmonic properties of gold nanoparticles separated from a gold mirror by an ultrathin oxide. *Nano Lett.* **12**, 2088–2094 (2012).

38. Hunger, R., Fritsche, R., Jaeckel, B. & Jaegermann, W. Chemical and electronic characterization of methyl-terminated Si (111) surfaces by high-resolution synchrotron photoelectron spectroscopy. *Phys. Rev. B.* **72**, 045317 (2005).

39. Haick, H., Hurley, P. T., Hochbaum, A. I., Yang, P. D. & Lewis, N. S. Electrical characteristics and chemical stability of non-oxidized, methyl-terminated silicon nanowires. *J. Am. Chem. Soc.* **128**, 8990–8991 (2006).

40. Reina, A. *et al.* Large area, few-layer graphene films on arbitrary substrates by chemical vapor deposition. *Nano Lett.* **9**, 30–35 (2009).

41. Palik, E. D. [Methods for determining optical parameters of thin films] *Handbook of optical constants of solids* 57–71 (Academic Press Inc., Boston, 1998).

42. Johnson, P. B. & Christy, R. W. Optical constants of the noble metals. *Phys. Rev. B* **6**, 4370–4379 (1972).

43. Chen, P. Y. & Alù, A. Atomically thin surface cloak using graphene monolayers. *ACS Nano* **5**, 5855–5863 (2011).

44. Gusynin, V. P., Sharapov, S. G. & Carbotte, J. P. Magneto-optical conductivity in graphene. *J. Phys.: Condens. Matter.* **19**, 026222 (2007).

45. Hanson, G. W. Quasi-transverse electromagnetic modes supported by a graphene parallel-plate waveguide. *J. Appl. Phys.* **104**, 084314–084315 (2008).

46. Hanson, G. W. Dyadic Green's functions and guided surface waves for a surface conductivity model of graphene. *J. Appl. Phys.* **103**, 064302–064308 (2008).

Acknowledgments

Author contributions

L.H.Z. and J.G.H. planned and performed the experiments, collected and analyzed the data, and wrote the paper. C.Y.W. and L.B.L. supervised the project, conceived the experiments, analyzed the results and wrote the paper. F.X.L., L.W., C.X., Y.Q.Y. and J.G.H. helped with synthesis of the materials and collected the data. All authors discussed the results and commented on the manuscript.

Additional information

Supplementary information accompanies this paper at http://www.nature.com/scientificreports

Competing financial interests: The authors declare no competing financial interests.

How to cite this article: Luo, L.-B. *et al.* Light trapping and surface plasmon enhanced high-performance NIR photodetector. *Sci. Rep.* **4**, 3914; DOI:10.1038/srep03914 (2014).